Motion Based Acceleration Correction for Improved Sensor Orientation Estimates

Terrell R. Bennett, Roozbeh Jafari, and Nicholas Gans
Jonsson School of Engineering
University of Texas at Dallas
Richardson, TX, USA

Abstract*— Inertial measurement units (IMUs) including accelerometers and gyroscopes are becoming very common and can be found in cell phones, fitness trackers, and other wearable devices. With the growth in wearable computing and body sensor networks, IMUs are also becoming more prevalent research environments for estimation and tracking of human motion. We demonstrate that the accelerometer angle estimate is inaccurate for typical motions and present a method using a kinematic model to correct the accelerometer angle estimate and improve overall orientation estimates using an extended Kalman filter (EKF). Our method improves upon the raw accelerometer orientation estimation method and a gyroscope based EKF method for sensor orientation during motion and at rest.

I. INTRODUCTION

Inertial measurement units (IMUs) including accelerometers and gyroscopes are becoming very common. They can be found in cell phones, fitness trackers, and other wearable devices. With the growth in wearable computing and body sensor networks, IMUs are also becoming more prevalent in research environments. They are used for movement and activity recognition [1, 2], rehabilitation [3, 4], localization [5, 6], and sports training [2, 7]. For many of these applications, accurate measurement of the orientation of limbs is critical for the application to work properly.

Systems that only have accelerometers use force measurements to estimate orientation of the joints using the gravity vector. While accelerometers measure acceleration due to motion as well as gravity, it can be useful to have these measurements decoupled. For example, having a motion-only acceleration measurement for a sensor attached to a golf club would allow mapping and analysis of a golf swing [8]. If a person wearing a sensor is walking or running, their speed could be estimated based on the accelerometer. On the other hand, gravity-only acceleration measurements could be useful for some health care applications. Posture or risk of falling could be determined while a person is in motion [9].

In accelerometer-only applications, it is often assumed that the subject is not moving during measurements, or that the gravity vector measured from the accelerometer will dominate any forces caused by body motion and provide an accurate orientation estimate. The accelerometer estimate works well when there is no motion, but when the system is in motion, it is not valid to ignore the acceleration that comes from motion. Gyroscope-only solutions estimate rotation well during motion but suffer from drift. This means the gyroscope estimate will slowly change over time due to integration error and the gyroscope's bias. We present a novel method which uses the gyroscope during motion to modify the accelerometer angle estimate to improve the overall estimate of orientation.

In this work, we use a kinematic model and an extended Kalman filter (EKF) to estimate the acceleration that an accelerometer will see due to movement. We subtract our motion based acceleration estimate from the measured acceleration. This modified acceleration is used to create an improved angle estimate, which is used to improve the orientation estimates of the entire system. Using a rigid double pendulum (*i.e.* Pendubot) to represent the human leg, we estimate the joint angles and improve the overall estimate of angle by correcting the accelerometer data and fusing it with the gyroscope data through an EKF. This solution involves using the gyroscope as well as an accelerometer which may increase system cost and power. Additionally, this solution requires a model to enable the acceleration correction. We mitigate these limitations by using a single chip solution with a gyroscope and accelerometer. In addition, we use a kinematic model based on the activity of interest to design our EKF.

Static measurements are sometimes used in body sensor networks to determine the initial orientation of sensors. In [10], Tundo et al. measure the gravity vector when there is no motion (*i.e.* the subject not moving) to estimate the orientation of a smartphone. This information is then used to reorient the measurements to a predetermined reference frame. This corrected orientation is used in activity detection but assumes there are no further orientation changes during motion. Friedman et al. also base their estimates of orientation on limited motion before and after a calibration movement [11]. These techniques allow for initial orientation estimates, but are not useful for estimates when the subject is in motion.

In [12], Mizell averages accelerometer readings over a fixed period to estimate the vertical acceleration due to gravity. Yao et al. design a real-time system for inclination sensing, which is also based on the concept that the net acceleration on the sensor over time is gravity [13]. Luinge et al. suggest that the gravitational acceleration has a larger magnitude relative to many human movements [14], and use the accelerometer angle estimate in a Kalman filter to improve orientation estimates. The assumption that gravity

978-1-4799-4959-5/14 $31.00 © 2014 IEEE
DOI 10.1109/BSN.2014.17

dominates the movement acceleration may be true if there are limited sensor positions (*i.e.* on the trunk and not limbs), and the subject is doing activities in which their posture and speed do not change dramatically or often. However, sensors attached to limbs are likely to see greater motion-based acceleration measurements, as we show in section V.

Liu et al. use two coaxial accelerometers on the same segment of the leg to reduce the effects of motion and improve angle estimates [15]. In [16], Wu et al. look to optimize the placement of one to eight sensors on a single rigid segment to improve the measurement of gravity for orientation detection. In these solutions, the sensors must be physically separated and processed for the accelerometer to provide additional information for orientation estimation. Additional sensors may not be feasible for certain situations and increase the processing necessary for the sensor network.

This paper is arranged as follows. Section II discusses theory behind using acceleration measurements for angle estimates. It also covers the kinematic model and how it relates to human motion. Section III describes the basics of the EKF and the state space model for our discussion. Section IV gives the details on the experimental set up and Section V gives an analysis of the results obtained. Finally, Section VI covers conclusions and future work.

II. Background and Kinematics

In [6], Bennett et al. used an EKF to estimate joint angles and estimate walking distance. The EKF used gyroscope measurements from two sensors to estimate the angle of the thigh and shin during walking. Gyroscopes drift over time, which reduces the accuracy of the estimate. To combat gyroscope drift and get additional data during more complex motions, accelerometers are commonly used [17, 18]. To use the accelerometer to assist in correcting angle estimates for the EKF, we model the acceleration that a sensor will see due to movement as well as due to gravity.

A. Acceleration Based Angle Estimates

For an accelerometer that is motionless, the sensor measurements will be directly related to the angle θ of the sensor relative to gravity. Using this knowledge, an orientation angle can be determined. A_x, which is the accelerometer measurement along the x-axis of the sensor, will be equal to $gcos\theta$, and A_y, which is the sensor y-axis accelerometer measurement, will be equal to $gsin\theta$. Using

$$\theta = atan2\left(\frac{A_y}{A_x}\right), \quad (1)$$

we can calculate θ based on the accelerometer measurements when the sensor is not moving.

When the sensor is in motion, the sensor still measures the acceleration of gravity. However, there are also acceleration components due to the motion of the sensor that contribute to the sensor measurements. Fig. 1 (a) shows the measured accelerations sum to give the gravitational acceleration (*i.e.* for a motionless sensor). Fig. 1 (b) shows that the sensor measurements for acceleration include motion based radial and tangential components, A_{rad} and A_{tan} respectively.

Ignoring the motion based acceleration will cause incorrect angle estimates because the sensor measurements are not due to gravity alone. If the motion based acceleration vectors can be determined, they can be removed from the accelerometer measurement leaving only the gravity-based acceleration. Following this, (1) can be used to as an improved estimate of the sensor angle.

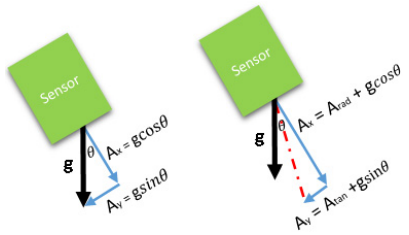

(a) (b)

Fig. 1: Accelerations seen by sensor with and without motion

B. Kinematics

As shown in our previous work, when walking in a straight line, the human leg can be modeled as a 2-link revolute robot with one link of the robot representing the femur and the second link representing the tibia/fibula. The revolute joints represent the hip and knee joints of the human leg. The Pendubot, as illustrated in Fig. 2, is a 2-link planar revolute robot (*i.e.* similar to the human leg while walking on a straight path). The joint at the base of link 1 is the origin of the inertial global frame for all estimates in the system. The x estimate is along the horizontal axis, and the y estimate is along the vertical axis. The angle θ_1 is measured with respect to the x-axis. We measure the angle of link 2 (θ_2) relative to link 1.

The Pendubot has fewer constraints on motion than the human leg (e.g. the "knee" can bend in either direction and the range of motion is larger). However, the Pendubot joints cannot twist, which allows a simpler model to be used. The Pendubot has optical encoders at each joint which are used in the experiments to give angle measurements with a resolution of 1000 cycles per revolution (CPR) (*i.e.* ±.18°).

The sensors are IMUs on the upper and lower links that measure the angular velocities and linear accelerations of the two links using gyroscopes and accelerometers respectively. In this system setup, the sensor attached to the second link will have greater orientation changes because link 2 sees all motion from link 1 and from its own movement and due to the increased movement of the second link during the walking motion. In addition, because the second link generally moves more than the first link, the acceleration forces from the movement will be greater. Because sensor 2 gives an angle estimate that contains information about θ_1 and θ_2 (*i.e.* the angle estimate from the

second sensor is($\theta_1 + \theta_2$)), we can use the data from this sensor to improve our estimates.

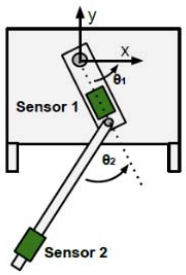

Fig. 2: Pendubot with a sensor on each link.

C. Acceleration Correction

As shown in [19], the equations for x displacement, y displacement and related derivatives in the base coordinate frame of a two link revolute robot are

$$x = a_1 c_1 + a_2 c_{12} \tag{2}$$

$$\dot{x} = -a_1 s_1 \dot{\theta}_1 - a_2 s_{12}\left(\dot{\theta}_1 + \dot{\theta}_2\right) \tag{3}$$

$$\ddot{x} = -a_1\left[c_1 \dot{\theta}_1^{\,2} + s_1 \ddot{\theta}_1\right] - a_2 c_{12}\left(\dot{\theta}_1 + \dot{\theta}_2\right)^2 - a_2 s_{12}\left(\ddot{\theta}_1 + \ddot{\theta}_2\right) \tag{4}$$

$$y = a_1 s_1 + a_2 s_{12} \tag{5}$$

$$\dot{y} = a_1 c_1 \dot{\theta}_1 + a_2 c_{12}\left(\dot{\theta}_1 + \dot{\theta}_2\right) \tag{6}$$

$$\ddot{y} = a_1\left[c_1 \ddot{\theta}_1 - s_1 \dot{\theta}_1^{\,2}\right] + a_2 c_{12}\left(\ddot{\theta}_1 + \ddot{\theta}_2\right) - a_2 s_{12}\left(\dot{\theta}_1 + \dot{\theta}_2\right)^2 \tag{7}$$

where a_1 is the length of the first link, a_2 is the length of the second link, $s_1 = \sin(\theta_1)$, $c_1 = \cos(\theta_1)$, $s_{12} = \sin(\theta_1 + \theta_2)$ and $c_{12} = cos(\theta_1 + \theta_2)$.

Based on (4) and (7) and using the signals estimated by the EKF described in Section III, we can estimate the acceleration that sensor 2 will see from motion in the global x and y coordinate frame. The sensor, however, has its own reference frame as shown in Fig. 3. The sensor 2 frame is not oriented the same as the global frame when the pendulum is at rest, and it is dynamic when the pendulum is in motion. Therefore, we use the rotation matrix

$$R_0^{S_2} = \begin{bmatrix} c_{12} & s_{12} & 0 \\ s_{12} & -c_{12} & 0 \\ 0 & 0 & -1 \end{bmatrix} \tag{8}$$

to rotate the measurements made in the global reference frame into the sensor 2 reference frame. The rotated estimates A_{tan} and A_{rad} are the tangential and radial components of the motion based acceleration respectively. These are found using (8) to rotate the results of (4) and (7).

Subtracting the tangential and radial acceleration estimates from the related sensor readings will leave an estimate of the gravity based acceleration on the sensor as

$$\begin{bmatrix} g_x \\ g_y \end{bmatrix} = \begin{bmatrix} A_x \\ A_y \end{bmatrix} - \begin{bmatrix} A_{rad} \\ A_{tan} \end{bmatrix}. \tag{9}$$

We then use the arctangent function on the estimated gravity vector to get an improved angle estimate that can be used to reduce the error in angle estimates due to gyroscope drift.

III. Extended Kalman Filter Model

In this section, we present the state space model and EKF considered in our system. The state vector is

$$\boldsymbol{x} = [x, y, \theta_1, \omega_1, \alpha_1, \theta_2, \omega_2, \alpha_2, \beta_1, \beta_2]^T \tag{10}$$

where θ_1 is the angle of the first joint, ω_1 is the angular velocity of the first joint, and α_1 is the corresponding angular acceleration. The angle, angular velocity, and angular acceleration of the second joint are θ_2, ω_2, and α_2 respectively. The biases from the gyroscope on the first sensor and gyroscope on the second sensor are β_1 and β_2 respectively. The biases are assumed to be constant or slowly time varying. Defining $A = -a_1 s_1 - a_2 s_{12}$, $B = -a_2 s_{12}$, $C = a_1 c_1 + a_2 c_{12}$, and $D = a_2 c_{12}$, we can take the derivative of (10) as $\dot{\boldsymbol{x}} = F\boldsymbol{x} + \boldsymbol{w}$, where $F \in \mathbb{R}^{10\times 10}$ is

$$F = \begin{bmatrix} 0 & 0 & 0 & A & 0 & 0 & B & 0 & 0 & 0 \\ 0 & 0 & 0 & C & 0 & 0 & D & 0 & 0 & 0 \\ 0 & 0 & 0 & 1 & 0 & 0 & 0 & 0 & 0 & 0 \\ 0 & 0 & 0 & 0 & 1 & 0 & 0 & 0 & 0 & 0 \\ 0 & 0 & 0 & 0 & 0 & 0 & 0 & 0 & 0 & 0 \\ 0 & 0 & 0 & 0 & 0 & 0 & 1 & 0 & 0 & 0 \\ 0 & 0 & 0 & 0 & 0 & 0 & 0 & 1 & 0 & 0 \\ 0 & 0 & 0 & 0 & 0 & 0 & 0 & 0 & 0 & 0 \\ 0 & 0 & 0 & 0 & 0 & 0 & 0 & 0 & 0 & 0 \\ 0 & 0 & 0 & 0 & 0 & 0 & 0 & 0 & 0 & 0 \end{bmatrix} \tag{11}$$

and $\boldsymbol{w}$ is a random process.

The measurement vector is given by $\boldsymbol{y}_k = [s_1, s_2, s_3] = [\omega_1 + \beta_1, \omega_1 + \omega_2 + \beta_2, \theta_1 + \theta_2]^T + \boldsymbol{v}$ where is $\boldsymbol{v}$ a random process, s_1 reflects the fact that the first link angular velocity measurement includes the first link rotation and the gyroscope 1 bias. Similarly, the lower link angular velocity measurement, s_2, is a combination of second link rotation, the first link rotation, and the bias of gyroscope 2 because the second link is connected to the first link. Finally, s_3 is the angle estimate from the accelerometer on sensor 2, which will see the total angular displacement of both links.

We implement a discrete time filter, and due to the trigonometric terms, we linearize the state equations at each iteration. Using the procedure outlined in [20], we approximate the discrete time system as

$$\Phi_k \approx I + FT_S \tag{12}$$

where T_S is the length of each time step and $I \in \mathbb{R}^{10\times 10}$ is the identity matrix. This leads to a discrete time state space model as in [21]

$$\boldsymbol{x}_{k+1} = \Phi_k \boldsymbol{x}_k + w_k \tag{13}$$

$$\boldsymbol{y}_k = H\boldsymbol{x}_k + v_k \tag{14}$$

where $k \in \{1,2,\dots\}$ is the discrete time index, $\boldsymbol{x}_k \in \mathbb{R}^{10}$ is the state vector at the time instant k, $\boldsymbol{y}_k \in \mathbb{R}^3$ is the measurement vector. $\Phi_k \in \mathbb{R}^{10\times10}$ is the state transition matrix that describes the progression of states over time and is described in (12). $H \in \mathbb{R}^{3\times10}$ is the matrix that relates the states to the measurements and is given by

$$H = \begin{bmatrix} 0 & 0 & 0 & 1 & 0 & 0 & 0 & 0 & 1 & 0 \\ 0 & 0 & 0 & 1 & 0 & 0 & 1 & 0 & 0 & 1 \\ 0 & 0 & 1 & 0 & 0 & 1 & 0 & 0 & 0 & 0 \end{bmatrix}. \tag{15}$$

The terms w_k and v_k are white, zero-mean Gaussian noise processes with covariance matrices $R \in \mathbb{R}^{3\times3}$ and $Q \in \mathbb{R}^{10\times10}$, given by

$$R = \begin{bmatrix} \sigma_1 & 0 & 0 \\ 0 & \sigma_2 & 0 \\ 0 & 0 & \sigma_3 \end{bmatrix} \tag{16}$$

$$\sigma_3 = \begin{Bmatrix} \sigma_s & |s_1 + s_2| < \delta \\ \sigma_f & else \end{Bmatrix} \tag{17}$$

$$Q = \begin{bmatrix} \sigma_d & 0 & 0 & 0 & 0 & 0 & 0 & 0 & 0 & 0 \\ 0 & \sigma_d & 0 & 0 & 0 & 0 & 0 & 0 & 0 & 0 \\ 0 & 0 & \frac{\sigma_{\theta_1}^9}{9} & \frac{\sigma_{\theta_1}^4}{4} & \frac{\sigma_{\theta_1}^5}{5} & 0 & 0 & 0 & 0 & 0 \\ 0 & 0 & \frac{\sigma_{\theta_1}^4}{4} & \frac{\sigma_{\theta_1}^3}{3} & \frac{\sigma_{\theta_1}^2}{2} & 0 & 0 & 0 & 0 & 0 \\ 0 & 0 & \frac{\sigma_{\theta_1}^5}{5} & \frac{\sigma_{\theta_1}^2}{2} & \sigma_{\theta_1} & 0 & 0 & 0 & 0 & 0 \\ 0 & 0 & 0 & 0 & 0 & \frac{\sigma_{\theta_2}^9}{9} & \frac{\sigma_{\theta_2}^4}{4} & \frac{\sigma_{\theta_2}^5}{5} & 0 & 0 \\ 0 & 0 & 0 & 0 & 0 & \frac{\sigma_{\theta_2}^4}{4} & \frac{\sigma_{\theta_2}^3}{3} & \frac{\sigma_{\theta_2}^2}{2} & 0 & 0 \\ 0 & 0 & 0 & 0 & 0 & \frac{\sigma_{\theta_2}^5}{5} & \frac{\sigma_{\theta_2}^2}{2} & \sigma_{\theta_2} & 0 & 0 \\ 0 & 0 & 0 & 0 & 0 & 0 & 0 & 0 & \sigma_\beta & 0 \\ 0 & 0 & 0 & 0 & 0 & 0 & 0 & 0 & 0 & \sigma_\beta \end{bmatrix} \tag{18}$$

The process noise matrix Q is constant with a block-diagonal structure. We model the process noise on the x, y, and β variables as independent, and the blocks for the $\theta_i, \omega_i, \alpha_i, i \in \{1,2\}$ reflect a random walk process. The $\sigma_d, \sigma_{\theta_1}, \sigma_{\theta_2}$, and σ_β terms in Q are determined by tuning for the best performance. The elements of R, σ_1 and σ_2, are constant and determined by taking the sample standard deviation of the measurement data during an initialization stage when the Pendubot is not in motion.

The noise term for σ_3 is dynamic as shown in (17). Based on s_1 and s_2, σ_3 toggles between σ_s and σ_f. In essence, the accelerometer is trusted more when the system is moving slower and less when the system is moving faster. The threshold, δ, determines when to adjust the noise level of the accelerometer. The parameters were chosen experimentally, but to test the robustness, we varied the variance parameters by $\pm10\%$ with no ill effects.

The EKF assumes that the state at the current time index evolves from the state from previous time index in a Markov process. The expected value of the state is derived from (13), providing the prediction stage of the EKF. It should also be noted that the state transition matrix must be updated at each time index. The equations corresponding to the prediction stage are given as

$$\boldsymbol{x}_{k+1|k}^- = \Phi_k \boldsymbol{x}_{k-1} \tag{19}$$

$$P_k^- = \Phi_k P_{k-1} \Phi_k^T + Q \tag{20}$$

where $P_k \in \mathbb{R}^{10\times10}$ is the estimate of the error covariance matrix at time k. After the prediction, the estimates are updated using the measurement. The equations involved in the update stage are

$$K_k = P_k^- H^T (H P_k^- H^T + R)^{-1} \tag{21}$$

$$\boldsymbol{x}_k = \boldsymbol{x}_k^- + K_k(\boldsymbol{y}_k - H\boldsymbol{x}_k^-) \tag{22}$$

$$P_k = (I - K_k H) P_k^- \tag{23}$$

where $K_k \in \mathbb{R}^{10\times10}$ is called the Kalman gain. Note that K_k weights the effects of the measurements as a function of the sensor noise and estimation error covariance matrices.

IV. Experiments

For each experiment, a sensor is placed on each of the two links of the Pendubot as shown in Fig. 2. They are aligned vertically and attached rigidly so that all rotation occurs about the z-axis of the sensor as shown in Fig. 3 (b).

Each trial begins and ends with the Pendubot at rest. This leads to initial state estimates $x = 0$m, $y = -(a_1 + a_2)$m, $\theta_1 = -\frac{pi}{2}$ radians, $\theta_2 = 0$ radians, $\omega_1 = 0\frac{radians}{second}$, $\omega_2 = 0\frac{radians}{second}$, $\beta_1 = \mu_1\frac{radians}{second}$, and $\beta_2 = \mu_2\frac{radians}{second}$ where $\mu_1 and\ \mu_2$ are the mean values of the gyroscopes collected during the first 2 seconds of the rest period before the Pendubot is moved. We attached a rigid stick to the Pendubot to keep the knee from hyperextending, and moved the links by hand to simulate human motion.

(a) (b)

Fig. 3: Custom Sensor & Sensor Axis Orientation

The sensors are custom-designed boards with an MPU9150, which has a 3-axis accelerometer and a 3-axis gyroscope. The accelerometer is set with a range of $\pm8g$. The gyroscopes have a full scale range of $\pm2000^o$ per second. The sensors collect the data and transfer it through a Bluetooth connection to a PC at ~200Hz. MATLAB is used to read and analyze the data.

Each sensor has its own clock and time stamps the data relative to the local clock. The data between the two sensors must be time synchronized. The sensor data is resampled

based on the local time stamps to correct for any minor deltas in the sampling frequency. After resampling, the sensors must be aligned for the signal processing. Because the two sensors are attached to the two links of the Pendubot, we align the sensor data based on the assumption that both sensors will see the initial motion at the same time. Using this assumption, we manually shift the data of the second sensor to match the first sensor. After synchronization, a median filter, over a window of 5 samples, is applied to the data to smooth any noise in the signal and handle any packet loss. Finally, all gyroscope data is converted to radians before applying the EKF.

In addition, the Pendubot was connected through USB to another PC that collected data from the two angle encoders through a LabView VI. The encoder data was collected at 200 Hz to serve as a gold standard for all angle estimates.

V. Analysis and Results

Fig. 4 shows the angle estimate based on the raw accelerometer readings (*i.e.* treating the acceleration vector as the direction of gravity) and the corrected acceleration angle estimate, with the encoder measurement. This movement was relatively slow, and the corrected acceleration angle estimate tracks the encoder measurement better than the estimate based on raw accelerometer measurements. This simple trial shows that the method for removing the motion based acceleration works. Due to the noise on the accelerometer signal, the correction will not be perfect, but the angle estimate does improve. The improvement can be seen with a root mean square error (RMSE) of 0.1163 radians for the corrected acceleration estimate versus 0.173 radians for the basic acceleration estimate over the trial.

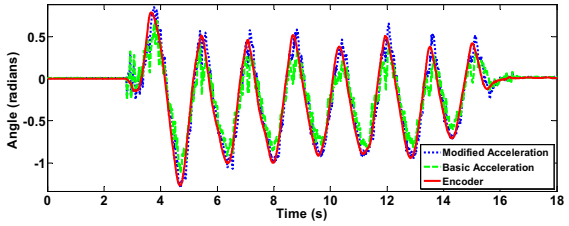

Fig. 4: Raw Acc. Angle Estimate vs Corrected Acc. Angle Estimate

Fig. 5 shows the encoder angle measurement for $\theta_1 + \theta_2$ and the accelerometer angle estimate from sensor 2 for an experiment with varying speed of motion. With faster movements, the acceleration angle estimate tracks the encoder measurement very poorly. When the motion slows or stops, the accelerometer angle estimate improves relative to the encoder. Over the entire trial, the accelerometer angle estimate has a RMSE of .718 radians.

Fig. 6 shows the same trial, but only uses the gyroscope measurements as inputs to the EKF to estimate the angle. During the faster motion, the system tracks well, but the drift in the gyroscope estimate causes error as the system slows and comes to rest as shown in the zoomed portion of Fig. 6. This offset will remain in the system and accumulate over time without some correction. As the system begins moving again, the estimate will already be incorrect due to the offset caused by the gyroscope drift. The gyroscope only EKF solution has a RMSE of 0.1011 radians over this trial.

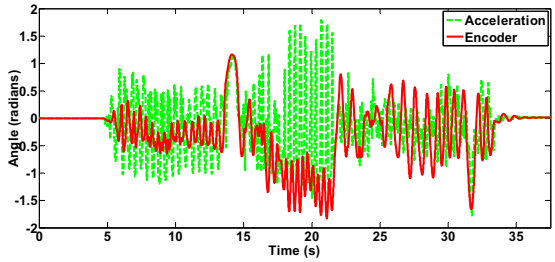

Fig. 5: Acceleration Angle Estimate vs. Encoder

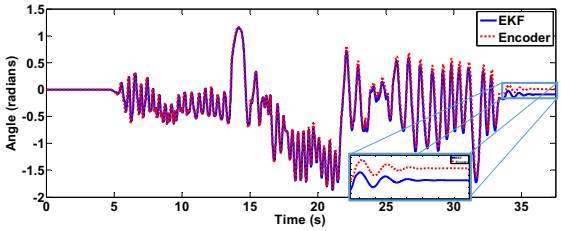

Fig. 6: Gyroscope only EKF vs. Encoder

Fig. 7 and Fig. 8 show the updated EKF using the raw accelerometer angle estimate, $[A_x\ A_y]^T$ as an input and using the corrected accelerometer vector $[g_x\ g_y]^T$ angle estimate as an input respectively. It can be seen that the updated EKF using the raw accelerometer angle estimate is an improvement over the accelerometer alone, but is not as accurate as the gyroscope alone. The EKF using the corrected accelerometer angle estimate tracks the encoder well during the motion, and reduces the error compared to the gyroscope only EKF during the periods without motion.

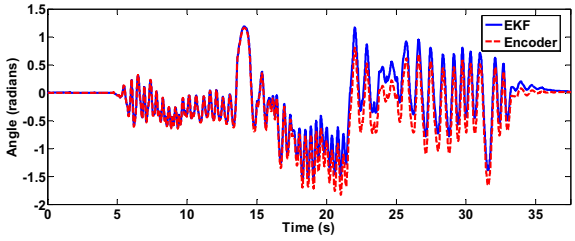

Fig. 7: EKF with Raw Accelerometer Angle Estimate vs Encoder

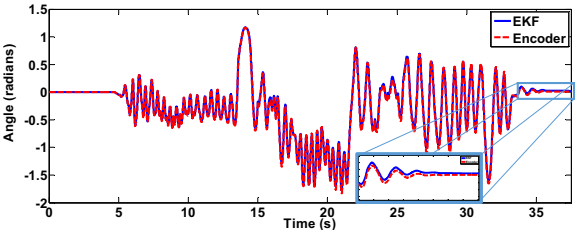

Fig. 8: EKF with Corrected Accelerometer Angle Estimate vs Encoder

The RMSE over the trial for the raw accelerometer EKF and the corrected accelerometer EKF are 0.1873 and 0.0306 radians respectively. The zoomed portion of Fig. 8 also shows that the EKF with the corrected accelerometer angle estimate improves the drift seen in the EKF which only uses the gyroscope. Over this trial, the proposed method has a RMSE that is about 70% smaller than the gyroscope only solution and 83% smaller than the RMSE of the EKF using the gyroscope and the raw acceleration data.

VI. Conclusion and Future Work

We have presented a novel method to correct acceleration based angle estimates, which are then used in an EKF to improve the overall estimate of the system. The method improves the estimate relative to a gyroscope-only EKF and an EKF using the raw acceleration angle estimate. The accelerometer and gyroscope measurements are used in an innovative way to not only mask the weakness of the other but to improve the data measurements. This method generated results that were more accurate than gyroscope only estimate methods, accelerometer only estimate methods, and combined sensor methods using the raw accelerometer data and the gyroscope. We also showed that accelerometers alone are not reliable as orientation sensors.

We plan to continue this work by automating the sensor synchronization. We currently use two sensors, but a larger network of sensors could be used. In these scenarios and in real time systems, synchronization would need to occur automatically. Additionally improving the motion model and the methods for selecting the model parameters could further improve the corrected acceleration angle estimates and allow us to model general human motions.

Acknowledgement

This work was supported in part by the National Science Foundation, under grant CNS-1150079 and the TerraSwarm, one of six centers of STARnet, a Semiconductor Research Corporation program sponsored by MARCO and DARPA. Any opinions, findings, conclusions, or recommendations expressed in this material are those of the authors and do not necessarily reflect the views of the funding organizations.

References

[1] P. H. Veltink, H. Bussmann, W. de Vries, W. Martens, R. C. Van Lummel, *et al.*, "Detection of static and dynamic activities using uniaxial accelerometers," *Rehabilitation Engineering, IEEE Transactions on*, vol. 4, no. 4, pp. 375–385, 1996.

[2] M. Ermes, J. Parkka, J. Mantyjarvi, and I. Korhonen, "Detection of daily activities and sports with wearable sensors in controlled and uncontrolled conditions," *Information Technology in Biomedicine, IEEE Transactions on*, vol. 12, no. 1, pp. 20–26, 2008.

[3] O. Giggins, D. Kelly, and B. Caulfield, "Evaluating rehabilitation exercise performance using a single inertial measurement unit," in *Proceedings of the 7th International Conference on Pervasive Computing Technologies for Healthcare*, pp. 49–56, ICST (Institute for Computer Sciences, Social-Informatics and Telecommunications Engineering), 2013.

[4] J. Lupinski, V. Menon, P. Roh, S. Yuen, A. Valdevit, and J. Andrish, "Measuring knee compliance to facilitate post-op ligament rehabilitation," in *Bioengineering Conference (NEBEC), 2011 IEEE 37th Annual Northeast*, pp. 1–2, IEEE, 2011.

[5] R. Zhang, F. Hoflinger, and L. Reindl, "Inertial sensor based indoor localization and monitoring system for emergency responders," *Sensors Journal, IEEE*, vol. 13, no. 2, pp. 838–848, 2013.

[6] T. Bennett, R. Jafari, and N. Gans, "An extended kalman filter to estimate human gait parameters and walking distance," in *American Control Conference (ACC)*, pp. 752–757, June 2013.

[7] V. Bonnet, C. Mazza, P. Fraisse, and A. Cappozzo, "Real-time estimate of body kinematics during a planar squat task using a single inertial measurement unit," *Biomedical Engineering, IEEE Transactions on*, vol. 60, no. 2, pp. 1920–1926, 2013.

[8] Y.-C. Huang, T.-L. Chen, B.-C. Chiu, C.-W. Yi, C.-W. Lin, Y.-J. Yeh, and L.-C. Kuo, "Calculate golf swing trajectories from imu sensing data," in *Parallel Processing Workshops (ICPPW), 2012 41st International Conference on*, pp. 505–513, IEEE, 2012.

[9] W.-S. Yeoh, I. Pek, Y.-H. Yong, X. Chen, and A. B. Waluyo, "Ambulatory monitoring of human posture and walking speed using wearable accelerometer sensors," in *Engineering in Medicine and Biology Society, 2008. EMBS 2008. 30th Annual International Conference of the IEEE*, pp. 5184–5187, IEEE, 2008.

[10] M. D. Tundo, E. Lemaire, and N. Baddour, "Correcting smartphone orientation for accelerometer-based analysis," in *Medical Measurements and Applications Proceedings (MeMeA), 2013 IEEE International Symposium on*, pp. 58–62, IEEE, 2013.

[11] A. Friedman, N. Hajj Chehade, C. Chien, and G. Pottie, "Estimation of accelerometer orientation for activity recognition," in *Engineering in Medicine and Biology Society (EMBC), 2012 Annual International Conference of the IEEE*, pp. 2076–2079, IEEE, 2012.

[12] D. Mizell, "Using gravity to estimate accelerometer orientation," in *Proceedings of the Seventh IEEE International Symposium on Wearable Computers (ISWC'03)*, vol. 1530, pp. 17–00, Citeseer, 2003.

[13] X. Yao, G. Sun, W.-Y. Lin, W.-C. Chou, K. F. Lei, and M.-Y. Lee, "The design of an in-line accelerometer-based inclination sensing system," in *Circuits and Systems (ISCAS), 2012 IEEE International Symposium on*, pp. 333–336, IEEE, 2012.

[14] H. Luinge, P. Veltink, and C. Baten, "Estimating orientation with gyroscopes and accelerometers," *Technology and health care*, vol. 7, no. 6, pp. 455–459, 1999.

[15] K. Liu, T. Liu, K. Shibata, Y. Inoue, and R. Zheng, "Novel approach for lower limb segment orientation in gait analysis using triaxial accelerometers," in *Advanced Intelligent Mechatronics, 2008. AIM 2008. IEEE/ASME International Conference on*, pp. 488–492, IEEE, 2008.

[16] C.-H. Wu, Y.-T. Chang, and Y.-C. Tseng, "On optimization of accelerometers deployment for human posture tracking," in *Body Sensor Networks (BSN), 2011 International Conference on*, pp. 186–190, IEEE, 2011.

[17] S.-h. Won, W. W. Melek, F. Golnaraghi, *et al.*, "A kalman/particle filter-based position and orientation estimation method using a position sensor/inertial measurement unit hybrid system," *Industrial Electronics, IEEE Transactions on*, vol. 57, no. 5, pp. 1787–1798, 2010.

[18] A. Young, "Comparison of orientation filter algorithms for realtime wireless inertial posture tracking," in *Wearable and Implantable Body Sensor Networks, 2009. BSN 2009. Sixth International Workshop on*, pp. 59–64, IEEE, 2009.

[19] M. W. Spong, S. Hutchinson, and M.Vidyasagar, *Robot Modelling and Control*. John Whiley and Sons, Inc, 2006.

[20] P. Zarchan and H. Musoff, *Fudamentals of Kalman Filtering: A Practical Approach, Third Edition*. AIAA, 2009.

[21] G. B. G. Welch, *An Introduction to the Kalman Filter*. University of North Carolina at Chapel Hill, NC, 2006.